Supporting information

Controlling Near-Surface Ni Composition in Octahedral PtNi(Mo) Nanoparticles by Mo Doping for a Highly Active Oxygen Reduction Reaction Catalyst

F. Dionigi,[‡] *C. Cesar Weber,*[‡] *M. Primbs,*[‡] *M. Gocyla,*[§] *A. Martinez Bonastre,*[▲] *C. Spöri,*[‡] *H. Schmies,*[‡] *E. Hornberger,*[‡] *S. Kühl,*[‡] *J. Drnec,*[ǁ] *M. Heggen,*[§] *J. Sharman,*[▲] *R. Edward Dunin-Borkowski,*[§] *P. Strasser*[*,‡,•]

[‡]The Electrochemical Energy, Catalysis, and Materials Science Laboratory, Department of Chemistry, Chemical Engineering Division, Technical University Berlin, 10623 Berlin, Germany.

[§]Ernst Ruska-Centre for Microscopy and Spectroscopy with Electrons, Forschungszentrum Jülich GmbH, 52425 Jülich, Germany.

[ǁ]European Synchrotron Radiation Facility, ID 31 Beamline, BP 220, F-38043 Grenoble Cedex, France.

[▲]Johnson Matthey Technology Centre, Blount's Court, Sonning Common, Reading, RG4 9NH, UK.

•Ertl Center for Electrochemistry and Catalysis Gwangju Institute of Science and Technology Gwangju 500–712, South Korea.

*Correspondence to: pstrasser@tu-berlin.de

Experimental part

Chemicals and materials

Platinum(II) acetylacetonate [$Pt(acac)_2$] (Pt 48.0% min) and nickel(II) acetylacetonate [$Ni(acac)_2$] (95%) were purchased from Alfa Aesar. Molybdenum hexacarbonyl (98%), benzoic acid (BA, ≥99.5%), N,N-dimethylformamide (DMF, 99.8%) were purchased from Sigma-Aldrich. Carbon Vulcan (XC72R) was purchased from Cabot. For the washing, ethanol (VWR, absolute, ≥99.8%), acetone (Sigma-Aldrich, ≥99.5%) and ultrapure water (Milli-Q, 18.2 MΩ) were used. All the chemicals were used as received without further purification.

Pt/C and d-PtNi/C

Pt/C and dealloyed PtNi/C (d-PtNi/C) with Pt-weight based loading on carbon of 50 Pt wt% and 28.6 Pt wt%, respectively, were provided by Johnson Matthey Fuel Cells Ltd (UK). Ni wt% of the d-PtNi/C was measured to be ~4.7 Ni wt%, resulting in the stoichiometry of $Pt_{65}Ni_{35}$.

Synthesis of oh-PtNi/C

In a typical synthesis of octahedral (oh-) shaped nanoparticles $Pt(acac)_2$ (64.0 mg, 162.8 μmol, 1.31 equiv. relative to $Ni(acac)_2$), $Ni(acac)_2$ (32.0 mg, 124.6 μmol, 1.00 equiv.) and benzoic

acid (488 mg, 4.00 mmol) were weighted into an autoclave glass liner with a magnetic stir bar. Parallel in a centrifuge vial, a suspension of Vulcan carbon (80 mg) in DMF (40 mL) was prepared by strong ultrasonication (Branson Sonifier® SLPe, for 15 min). The suspension was added to the autoclave glass liner and the mixture was put in an ultrasonic bath for 18 min. Afterwards, it was transferred into an autoclave (100 ml/100 bar Model I Roth) and hermetically sealed with a polytetrafluoroethylene (PTFE) ring. The autoclave was heated to 160 °C for 12 hours while stirring the mixture during the whole solvothermal treatment. The autoclave was cooled down to room temperature overnight and the washing procedure was carried out. The composition of the as prepared catalyst was $Pt_{71.4}Ni_{28.6}$ and the Pt-based weight loading was 21.5 Pt wt%.

Synthesis of oh-PtNi(Mo)/C

The synthesis of PtNi(Mo)/C, as the previously described synthesis of PtNi/C, was adapted and upscaled from Huang et al.[1] PtNi(Mo)/C catalyst was obtained by surface doping of already preformed PtNi/C-nanoparticles. For the growth of the PtNi/C (step 1), the amount of metal precursors were rescaled to obtain a final Pt-weight based loading on carbon support which was similar for PtNi/C and PtNi(Mo)/C. 48 mg of $Pt(acac)_2$, 24 mg of $Ni(acac)_2$ and 366 mg of BA were used (equivalent to a rescaling factor of 0.75), while DMF and carbon amounts were unaltered. After the solvothermal treatment of the PtNi/C particles described above, the autoclave was opened and $Pt(acac)_2$ (12.0 mg, 30.5 µmol), $Ni(acac)_2$ (6.0 mg, 23.3 µmol) and $Mo(CO)_6$ (4.8 mg) were weighted into the autoclave glass liner containing the unwashed nanoparticle suspension. 5 ml of DMF was added to compensate for solvent evaporation which after cooling was found inside the stainless-steel autoclave but outside the glass liner. The mixture was ultrasonicated (sonication bath) for 40 min. Afterwards it was transferred to the autoclave and the mixture was heated to 170 °C for 48 hours. The autoclave was cooled down to room temperature overnight and the washing procedure was carried out.

The composition of the as prepared catalysts was $Pt_{66.6}Ni_{31.9}Mo_{1.5}$ and the Pt-based weight loading was 17.9 Pt wt%.

Synthesis variations: oh-PtNi/C-2steps and oh-PtNi(Mo)/C-30wt%

The synthesis of oh-PtNi/C-2steps was conducted following the one of oh-PtNi(Mo)/C with the only difference being the omission of the $Mo(CO)_6$ precursor. The obtained catalyst showed a composition of $Pt_{68.6}Ni_{31.4}$ and a Pt weight loading on carbon support of 18.9 Pt wt%, both obtained by ICP-OES.

Oh-PtNi(Mo)/C-30wt% was obtained by surface doping PtNi/C nanoparticles which were synthesized with condition identical to PtNi/C (so without the rescaling factor of 0.75). During the second step, $Pt(acac)_2$ (16.0 mg, 40.7 μmol), $Ni(acac)_2$ (8.0 mg, 31.1 μmol) and $Mo(CO)_6$ (3.2 mg) were added. Due to differences in the amount of precursors respect to the optimized oh-PtNi(Mo)/C, the loading was 29.7 Pt wt%, so higher than the one of the other octahedral catalysts considered in this work. The final composition was $Pt_{67.5}Ni_{31.6}Mo_{0.9}$.

Washing procedure:

After cooling naturally down to room temperature (~ 5 hours), the autoclave was opened and the suspension in the glass liner was placed in an ultrasonication bath for 5 min. The suspension was divided into two 50 mL centrifuge vials and 15 mL EtOH and 5 mL acetone were added into each vial. After ultrasonication (5 min), the suspension was centrifuged (15 min, 8500 rpm). The solvent was discarded and the particles were again suspended in EtOH (16 mL) and acetone (16 mL) by ultrasonication. After centrifugation (15 min, 8500 rpm), the solvents were discarded and the washing procedure was repeated with $EtOH/H_2O$ (32 mL,

1:1) and ultrapure water (32 mL). After the last washing step, the particles were freeze dried overnight.

Synthesis of catalyst for fuel cell testing

For fuel cell testing the amount of 1 g of catalyst was required by an established ink preparation procedure. A scale up effort was necessary since our synthesis procedure for RDE testing produces ~100 mg of catalyst per batch. Scaling up a synthesis is particularly challenging, i.e. in avoiding inhomogeneous thermal and compositional distributions when using larger volume.[2] Therefore we choose to replicate the synthesis by the times necessary to reach 1 g of catalyst. 13 batches were produced and the elemental composition and Pt based weight loading on carbon were analyzed by inductively-coupled plasma optical emission spectroscopy (ICP-OES) for each batch (Figure S26). Two batches were discarded being the two that more deviated from the composition of the most active oh-PtNi(Mo)/C. The mass of the selected batches reached the value of 1110 mg. Overall, good reproducibility in composition and loading is observed among the batches. The Pt content varied between 62.7 at% and 69.3 at% while the Pt based weight loading between 18 Pt wt% and 23 Pt wt%. The mass-weighted average composition was $Pt_{65.2}Ni_{33.5}Mo_{1.3}$ and the Pt based weight loading was 20.56 Pt wt%.

Physico-chemical Characterization

XRD: X-ray powder diffraction (XRD) patterns were collected using a D8 Advance-Diffractometer (Bruker) equipped with a Lynx Eye Detector and KFL Cu 2K X-ray tube. The measurement was carried out at a step size of 0.04°, in a 2θ-Range between 20 and 90°.

ICP OES: The atomic composition of the different catalysts was determined by inductively coupled plasma mass spectroscopy (ICP-MS) using a 715-ES-ICP analysis system (Varian).

The samples were prepared by dissolving the catalysts powders in a mixture of H2SO4, HNO3 and HCl (1:1:3). The solutions were heated from room temperature to 180 °C in 10 min using a Microwave Discover SP-D (CEM corporation), keeping at this temperature during 20 min. Finally, the cooled solutions were diluted with MilliQ water, filtered and taken to a known volume. To estimate the concentration of the solution, 5 standards of Pt, Ni and Mo with a concentration of 0, 1, 4, 7 and 12 mg/l of each element were prepared. The concentration of each element was taken from one specific wavelength to achieve comparable results. Platinum concentration was taken at 265.945 nm, nickel at 231.604 nm, and molybdenum at 268.414 nm.

TEM: Transmission electron microscopy (TEM) images were recorded on a FEI Tecnai G2 20 S-TWIN with a LaB_6 cathode operating with 200 kV acceleration voltage and a resolution limit of 0.24 nm. Samples were dispersed in ethanol with an ultrasonic horn (~15 min), drop casted on a Cu grid (400 mesh), and dried in air at 60 °C for 10 min.

XRF: X-Ray fluorescence (XRF) spectra were obtained on an S8 Tiger WDXRF spectrometer (Bruker AXS GmbH, Germany) equipped with a 3 kW rhodium X-ray source. The Pt Lα and Ni Kα lines were calibrated to reference samples of the same geometry and structure with known composition. Mo content in all samples was below the detection limit of XRF and as such neglected for the analysis. All measured samples consist of the same principle composition and setup as the in-situ WAXS samples (a droplet of catalyst ink on a carbon paper, see Fig. S15). The multi-layer-analysis tool MLQuant (BrukerAXS GmbH, Germany) was employed for the measurement evaluation. The applied multi-layer model comprises of a carbon matrix (the carbon paper holding the catalyst drop) as substrate layer as well as a catalyst layer of Pt, Ni and C (for the carbon support).

SEM: SEM/EDX was conducted on a JEOL 7401F field emission scanning electron microscope operated at 10 kV. Images were acquired in secondary electron mode. EDX

spectra were acquired with a Quantax 400 detector (BrukerAXS Microanalysis GmbH, Germany) attached to the JEOL 7401F. EDX spectra were evaluated with the Esprit software package (Bruker, Germany).

3D models were represented by using VESTA program.[3]

Scanning transmission electron microscopy (STEM): STEM was performed using a Cs-probe corrected FEI Titan 80-200 ("ChemiSTEM") microscope which was operated at 200 kV. In order to achieve "Z-Contrast" conditions, a probe semi-angle of 25 mrad and an inner collection semi-angle of the detector of 88 mrad were used. Compositional maps were obtained with energy-dispersive X-ray spectroscopy (EDX) using four large-solid-angle symmetrical Si drift detectors. For EDX elemental mapping, Pt L, Ni K and Mo K peaks were used. The error of the EDX composition measurement for individual particles after a typical investigation of 15 minutes is about +/- 2 at.%.

Catalyst ink preparation:

The catalyst inks for electrochemical measurements were prepared by following the guidelines included in a recently published protocol.[4] The amount of catalyst to target a specific Pt loading was added to a solution of 3.98 ml ultrapure water, 1 ml isopropanol and an aliquot of a 5 wt% Nafion ionomer solution (Sigma-Aldrich). The amount of Nafion was varied for different target loadings, typically 10 µl was added for 10 $\mu g_{Pt}/cm^2$ and 20 µl for 20 $\mu g_{Pt}/cm^2$ or intermediate loadings. The suspension was then sonicated with an ultrasonic horn sonicator (Branson Sonifier 150) for 15-30 min while immersed in a water bath. The ink was used on the same day. An aliquot of the ink was drop casted by a pipette on a glassy carbon (GC) rotating disk electrode (diameter Ø=5 mm). The film was dried at 60°C for 7 minutes. For Pt/C and d-PtNi/C the loading of 20 $\mu g_{Pt}/cm^2$ was targeted after being selected as optimal

in a preliminary screening.[4] For oh-PtNi(Mo), due to the high activity and current at 0.9 V vs RHE close to the diffusion limited current, a lower loading was attempted. For this catalyst, 10 $\mu g_{Pt}/cm^2$ was found to be the minimum loading necessary to obtain a uniform layer on the GC, and therefore selected also for the other octahedral catalysts. For oh-PtNi/C, the loadings of 10 and 20 $\mu g_{Pt}/cm^2$ were compared and the initial activity was reproduced within the error.

Electrochemical Characterization, CO stripping, activity and stability test by RDE:

For electrochemical characterizations a conventional three electrode cell with a Pt mesh as counter electrode, a reference Mercury/Mercury(I) sulfate electrode (MMS, Hg/Hg_2SO_4) in a Luggin capillary and a GC working electrode (5 mm diameter) was used. The working electrode was controlled by a rotator from Pine Research Instrumentation. The reference electrode was calibrated regularly using a homemade reversible hydrogen electrode (RHE) obtained using a polycrystalline Pt disk and bubbling hydrogen. All potentials in this paper are referred to RHE. A 0.1 M $HClO_4$ was used for electrochemical measurements (diluted from 70 % conc. $HClO_4$, 99.999 % trace metal bases, Sigma Aldrich with milli-Q water). All measurements were performed with a BioLogics Science Instruments potentiostat model SP-150 and VSP. The degree of purity for the used gases was 99.998 % for oxygen, 99.999 % for nitrogen and 99.999 % for hydrogen.

The electrochemical protocol was adapted from Martens et al.[4]

Activation Step: The working electrode was lowered into the N_2 saturated electrolyte under potential control at 0.05 V vs. RHE and under rotation at 1600 rpm to prevent bubbles to be trapped on the catalyst film. Rotation was then turned off. 50 potential cycles from 0.05 to 0.925 V vs. RHE at the scan rate of v = 100 mVs^{-1} and without rotation were applied, since they were found sufficient to reach a stable cyclic voltammogram curve. Then 3 cycles were

applied within the same potential range but at 20 mV s^{-1}. The third cycle was used to evaluate the electrochemical catalyst surface area (ECSA) from hydrogen under potential deposition (H_{upd}).

H_{upd}-ECSA evaluation: The H_{upd}-ECSA was determined by integrating the background-subtracted current in the negative going sweep between an upper potential limit where the cathodic current corresponds to the capacitive background current and a lower potential limit, taken as the potential of "minimum current" before onset of the hydrogen evolution reaction (HER), assuming a value of 210 μC cm^{-2} for adsorption of a hydrogen monolayer and normalizing by the scan rate. Note that in the text the mass normalized ECSA, which correspond to the ECSA normalized by the Pt mass loading on the electrode, is denoted as ECSA for simplicity.

Impedance Spectroscopy: The presented results are iR corrected after the measurements, where the resistance R was determined by potential electrochemical impedance spectroscopy. A potential of 0.5 V vs RHE was applied for 1 minute. Then an impedance measurement was performed by applying an AC amplitude of 10 mV and frequency from 100'000 Hz to 10 Hz at 0.5 V vs RHE. The resistance R was then determined from the Im (Z) vs. Re (Z) plot.

ORR testing: ORR testing was performed after carrying out the activation and impedance spectroscopy. First, the background current was determined. The rotation was set to 1600 rpm, and the potential of 0.05 V was applied for 30 s in N_2 saturated electrolyte. Then a linear scan at 20 mV s^{-1} was applied till the upper potential of 1.0 V vs RHE. The scan was repeated once. Then the electrode was raised and O_2 was bubbled for 30 minutes, after which O_2 was vented above the electrolyte. Quickly after stopping bubbling, the electrode was then inserted at 0.05 V vs RHE and this potential hold for 30 s. The same linear scan was applied (0.05 V-1.0 V vs RHE, 20 mV s^{-1}) and the measurement repeated two times. We note that the scan rate

has an influence on the mass normalized current, i.e. at higher scan rate a higher performance is usually reported. In our previous benchmarking paper we addressed this issue referring to the literature.[4] In general scan rates in the range 10-20 mV s^{-1} are recommended, as not too high, so that capacitive currents are minimised and possible overcorrection avoided, and neither too low, in which case the amount of OH_{ads} on the surface and impurity adsorption might be large and decrease the activity.

Analysis of ORR activity: First the potentials were iR corrected. Then the ORR current, i_{ORR}, was determined at 0.9 V vs RHE by subtraction of the background scan, performed in N_2 saturated electrolyte, from the scan performed in O_2 saturated electrolyte. In a similar way the true limiting current i_L was obtained by subtracting the current in N_2 saturated electrolyte at the potential where the contribution is purely capacitive (i.e. 0.4 V vs RHE) to the diffusion limiting current measured during the scan in O_2 saturated electrolyte. Finally the kinetic current i_k was calculated by the Koutecky-Levich equation. The mass activity was calculated by dividing i_k by the Pt mass loading on the electrode and the specific activity was calculated by dividing i_k by the H_{upd}-ECSA.

Stability testing (RDE protocol): The stability test was performed after carrying out the activation, impedance measurement and activity measurements. The rotation was turned off, the electrode raised from the electrolyte under potential control and N_2 was bubbled for 20-30 min. Then the electrode was reinserted and the potential cycled between 0.6 and 0.925 V vs RHE at 100 mVs^{-1} for 10'000 cycles, while venting above the electrolyte with N_2. After that the potential was cycled as described in "activation", but only 3 times at 100 $mVs^{-1}$and 3 times at 20 mVs^{-1}. Then *impedance spectroscopy* and the *ORR testing* procedure were performed.

CO stripping: CO stripping experiments were performed following activation treatment. After the activation, 0.05 V vs RHE was applied and the rotation was set to 400 rpm while bubbling

N_2 for 10 min. Then CO was bubbled for another 10 min at the same rotation speed. The gas was switched back to N_2 and the electrolyte was bubbled for another 10 min to remove CO. Then the rotation was turned off and five cyclic voltammetry cycles were recorded at 20 mV s^{-1} between 0.05 V vs RHE and 1 V vs RHE, while venting N_2 above the electrolyte.

Analysis of CO stripping: The CO stripping data were analyzed to calculate the CO-ECSA, the ratio of CO-ECSA/H_{upd}-ECSA and to determine the average CO stripping peak position. For the CO-ECSA, the positive scan of the cycle after the CO stripping was used as background and subtracted from the positive scan of the CO stripping curve. Then the integral of the peak was calculated in the iR corrected potential range from the crossing of the curves to the highest potential (~1 V vs RHE). Finally, the CO-ECSA was calculated assuming a value of 420 μC cm^{-2} for the electrooxidation of a monolayer of adsorbed CO and normalizing by the scan rate. The H_{upd}-ECSA after CO stripping was calculated as previously described for standard H_{upd}-ECSA, using the cycle after CO stripping. To show that the CO stripping curve is composed of multiple contributions, the background subtracted CO stripping curves were fitted with Pseudo-Voigt functions in the potential range from 0.4 to 1.0 V vs RHE. The CO stripping was further analyzed by calculating the first moment of the potential weight of the CO stripping voltammogram in the potential range from 0.55 to 1 V vs RHE.[5, 6] Briefly, the current of the background subtracted CO stripping curves were multiplied by the corresponding voltage and integrated in this potential range. Finally, this integral was normalized by the one obtained by integration of the currents in the same potential range.

In situ WAXS:

For the *in situ* WAXS experiments, oh-PtNi/C and oh-PtNi(Mo)/C catalysts were deposited by drop casting from an ink on a carbon paper stripe which was previously cut from a gas

diffusion layer (GDL) sheet (28BC, SIGRACET®, SGL group) (Figure S15a). The amount of catalyst deposited, ~ 9.8 μg_{Pt}, is five times the one used for thin film RDE experiments. After drying in an oven, the edge of the GDL stripe far from the sample was wrapped with copper tape and electrically contacted by a crocodile clip in order to be used as the working electrode. A Pt wire was used as counter electrode and a Ag/AgCl electrode, previously calibrated versus a reversible hydrogen electrode, as reference electrode. The electrolyte was 0.1 M $HClO_4$, and was injected with a pipette in a home-made PEEK cell (Figure S15b) which had two openings covered by PEEK foil as X-Ray windows.

The samples were measured after inserting the electrolyte (wet state), after activation by the same protocol used in RDE experiments (activated state) and during and after stability test. Two stability protocols were investigated and schematically illustrated in Figure 4a. Both stability tests were performed after a fresh sample was activated. One protocol (L-stability, where "L" stands for low potential) was designed to simulate life-time operation, where exposure to high anodic potentials is prevented, and was simply the stability protocol used in RDE experiments but with half the number of cycles. The other stability protocol (H-stability, where "h" stands for high potential) was designed to consider the effects of start-up/shut-down, where high anodic potentials can be reached. The upper potential was increased to 1.26 V_{RHE} and, to last roughly the same of the other one, the number of cycles was further halved. During operation the electrolyte was in equilibrium with air.

Investigation of crystal structure under electrochemical reaction conditions have been conducted at the ID31 beamline of the European Synchrotron Radiation Facility (ESRF) in Grenoble (Fr). Diffraction patterns were recorded using a monochromatized X-ray beam in the range 78.0-78.6 KeV focused to 20 × 5 μm^2 and a large area Pilatus3X CdTe 2M detector. The 2D WAXS images recorded by the detector were then radially integrated using a pyFAI code [https://doi.org/10.1107/S1600576715004306]. Diffraction patterns were corrected by

the background, by subtracting a WAXS pattern obtained in a point of the GDL where no sample was present. The working distance was calibrated using a CeO_2 standard (NIST SRM 674b). Electrochemical protocols were applied using a SP-200 Potenstiotat (BioLogic Instruments).

Rietveld refinement:

Rietveld refinement was performed using the software Topas 4.2 by Bruker AXS Inc.

Fuel cell testing:

The membrane electrode assembly (MEA) fabrication procedures and operating conditions were the same as in ref.[4].

MEA fabrication

The membrane electrode assemblies (MEAs) used in this work consist of five layers. Nafion 1100EW (equivalent weight in g polymer/mol H^+) was used to fabricate thin-layer electrodes. The cathode catalyst layers were prepared at an ionomer/carbon weight ratio of ca. 0.8/1 and metal loadings of ca 0.10 and 0.20 mg_{Pt} cm^{-2}. The anode catalyst layer was kept constant at an ionomer/carbon weight ratio of ca. 1.5/1 and a metal loading of 0.1 mg_{Pt} cm^{-2}. The membrane used was a perfluorosulfonic acid type, fabricated at JMFC with a thickness of ca. 20 μm. Catalyst layers were produced on a PTFE substrate and transferred via a decal method onto the membrane. Single cells (50 cm^2 active area) were assembled by sandwiching the catalyst coated membranes between the GDLs and applying an average compression onto the active area.

MEA operating conditions

The fuel cell station was built in-house at JMFC. Pure oxygen and synthetic air were used as cathode reactants and pure H_2 as the anode reactant (all gases of 99.9% purity). Stoichiometric flow rates of anode (s = 2) and cathode (s = 9.5 for O_2 and s = 2 for air) reactants were used at current densities >0.2 A cm^{-2} and constant flows (corresponding to 0.2

A cm^{-2} flows) at <0.2 A cm^{-2}. Reactant humidification was achieved by water-bubblers, the temperatures of which were calibrated to yield the desired relative humidity (RH) values. Humidity and cell pressure were measured at the inlet for both electrodes. Cell resistances as a function of current density (i.e., the sum of the proton-conduction resistance in the membrane and the various electronic resistances, bulk and contact resistances) were determined using an AC perturbation of 1 kHz at three different current densities of 25, 50 and 100 mA cm^{-2} and also using a current interrupt method. For each data point, the cell voltage was stabilized for 4 min where the current was measured. Multiple-path serpentine flow-fields (two and three parallel channels for the anode and cathode, respectively) machined into sealed graphite blocks were used for testing.

The MEAs were conditioned by the application of a constant current density of 500 mA cm^{-2} under H_2/Air at 50 kPa gauge, 100% RH and 80°C. The cell voltage was monitored until a stable value was observed. The conditioning step lasted 2h unless specified otherwise. Afterwards the cathode catalyst layer was exposed to a series of cathode starvation steps followed by 2h current hold at 500 mA cm^{-2} until a stable voltage was observed. The cathode starvation step (purging of cathode compartment with pure nitrogen) reduces the cathode voltage to below 0.1V and it is intended to provide an electrochemical cleaning step for the cathode catalyst before measuring its activity under H_2/O_2 [7]. After the starvation steps the MEA was ready for testing by H_2/O_2 polarisation curves for MA quantification (50 kPa_{gauge}, 100% RH and 80°C). The polarisation curves were recorded from low (i.e. 0.05 Acm^{-2}) to high current (i.e. 2 A cm^{-2}) ascending direction and backwards, descending direction. The lower current density limit was determined by maintaining the stoichiometry, at even lower currents there would be a risk of working under over-stoichiometric conditions with the used setup. The current density was maintained for 3 minutes at each step and the MA value was obtained from the ascending polarisation curve at 0.9 V by extrapolation, after correction for the cell ohmic resistance. For this study, H_2-crossover current densities were measured using

the procedure described by Kocha et al. [1]. In this test the hydrogen that permeates through the membrane to the cathode is oxidized by the application of a voltage (typically 250-300 mV are sufficient, and the latest above 400 mV one is in the mass transport limit [8]) and the resulting current measured. Therefore the cell was operated under H_2/N_2 and the gas crossover measurements were done at each of the operating conditions (*i.e.*, temperature and H_2-partial pressure). The catalyst mass activity was not corrected on the basis of H_2-crossover current densities, i_{eff} (i.e., $i_{eff} = i + ix$). Under the conditions used in this work *ix* was on the order of 2–5 A cm^{-2}. Performance curves in 50 cm^2 single cells were done with a three way switch polarization curves in H_2 / (O_2, Helox and Air) at 100 $kPa_{gauge\text{-}inlet}$ and 80 °C. The cell current density was held for 10 min at each point and the cell voltage was averaged on the last minute. Cell performance in H_2/Air is plotted in the descending direction, from low currents to high currents. The cell resistance was calculated from the intercept at high frequency and the values obtained were 60±2 mOhm cm at 100 $kPa_{gauge\text{-}inlet}$ and 80 °C. Performance in H_2/Air was not *i*R corrected.

The ECSA was measured with the CO stripping method using the cell in half cell mode where the anode electrode acts as a pseudo reference electrode. The cathode voltage was controlled at 0.125 V at 80°C, 100% RH and 50 kPa_{gauge} whilst purging with 1% CO in N_2 at 300 ml min^{-1} for 15 min. Afterwards the cathode was purged with N_2 at the same flow rate for 2 h to ensure that CO is removed from the bubblers and the catalyst layer pores. The adsorbed CO is oxidised electrochemically by scanning the cathode voltage from 0.125 V to 0.85 V and back to 0.05 V, at 20 mV s^{-1} for three cycles. The area under the CO oxidation peak is integrated by subtracting the third scan from the first scan and using a 420 μC cm^{-2} constant for a CO monolayer on Pt [9, 10].

Additional information

CO stripping study with rotating disk electrode

CO stripping is an *in situ* surface sensitive method and activity relations with certain properties of the surfaces determined by CO stripping were reported for some catalyst systems.[5, 6, 11] Two important parameters are often discussed in the literature:[5, 6, 12-20] the area, from which the CO-ECSA can be derived, and the peak position, which strongly depends on the CO oxidation mechanism. The ECSA determined by CO stripping is similar to the H_{upd}-ECSA for Pt/C, but it is higher than the latter one for the other Ni containing catalysts (Figure S7). This behavior is in agreement with literature reports on the effect of Ni on the determination of ECSA.[13] While for some specific systems the ratio of the CO-ECSA/H_{upd}-ECSA was reported to give indication for active catalysts,[11] this is not the case in our experiments, since a clear correlation cannot be established. This is in agreement with a recent work where CO stripping experiments were conducted in a single cell with membrane electrode assembly (MEA).[19] However, in agreement with previous work,[11, 19] we believe that this ratio can still be used to identify subsurface effect derived by the presence of Ni, i.e. d-PtNi/C, oh-PtNi/C and oh-PtNi(Mo)/C show improved activity in comparison to Pt/C and their CO-ECSA/H_{upd}-ECSA ratio clearly departs from 1. The CO stripping curves obtained after activation and subtracted from the background scans are shown in Figure S8 for Pt/C, d-PtNi/C, oh-PtNi/C, oh-PtNi(Mo)/C. All profiles can be deconvoluted in at least two peaks by fitting using multiple pseudo-Voigt functions. Both commercial Pt/C and d-PtNi/C shows the major component centered at ~ 0.80 V_{RHE}, with a small shoulder at 0.71 V_{RHE}, more pronounced for d-PtNi/C. Interpretation of the single peaks, especially of the lower potential shoulder, is not simple due to multiple dependences of the peak position i.e. nanoparticle agglomeration and surface defects as shown for Pt/C.[16, 17] These effects might play a minor role for PtNi alloys respect to effects due to the presence of the non noble metal,[14] and, assuming this hypothesis, the cathodic shift of CO stripping peaks can be interpreted as the

result of a Ni (or Co) richer surface.[14, 15] Indeed, both CO stripping peaks of oh-PtNi/C and oh-PtNi(Mo)/C, where Ni composition is ~ 30 at% and no specific Ni leaching or dealloying procedure has been applied besides activation, are considerably cathodically shifted respect to the other two catalysts. In general two main contributions can be assigned: a peak at 0.75 V_{RHE} and a peak centered at ~ 0.69 $V_{RHE,}$ which might be further deconvoluted in more overlapping peaks, as clearly visible for oh-PtNi/C. By changing the activation protocol, using a higher upper potential limit during cycling, we noticed that the ratio of the two contributions of the CO stripping curve changes (Figure S9). Therefore the center of the CO stripping peaks depends on the activation protocol, and comparison with other reports in the literatures has to be done with care if the protocols differ. For oh-PtNi/C the component at 0.75 V_{RHE} is more enhanced when the upper potential in the activation is increased from 0.925 V_{RHE} to 1.0 V_{RHE}, in agreement with this peak being the main component for similar element anisotropic PtNi octahedral catalysts reported by our group where the same upper potential was used.[7, 15] The onset of the CO stripping peaks is slightly more cathodic for oh-PtNi/C respect to oh-PtNi(Mo)/C, however, as shown by comparing two extra samples with slightly different compositions (Figure S10), the differences are within 20 mV and appear to be too small to attempt a correlation with activity, which differs up to a factor 2. The average CO stripping potential can be discussed as proposed by Chattot *et al.*[5] by calculating the first moment of the potential weight of the CO stripping voltammogram between a defined potential range (Figure S11a), or, in other words, the weighted mean of the recorded potentials in a certain potential range using the module of the currents as weights. This was shown to correlate linearly with the specific activity (SA) for hollow PtNi nanoparticles of Ni content between 14 and 23 at%.[6] For the catalysts analyzed in the work presented here, especially among the catalysts with octahedral nanoparticles which have very similar Ni composition (~30 at%), a clear correlation explaining the difference in ORR activity was not observed (Figure S11b). Therefore, we conclude that, in agreement with experiments conducted in single cell with

membrane electrode assembly (MEA),[19] not all subsurface effects that are important for ORR are strongly reflected in CO stripping experiments.

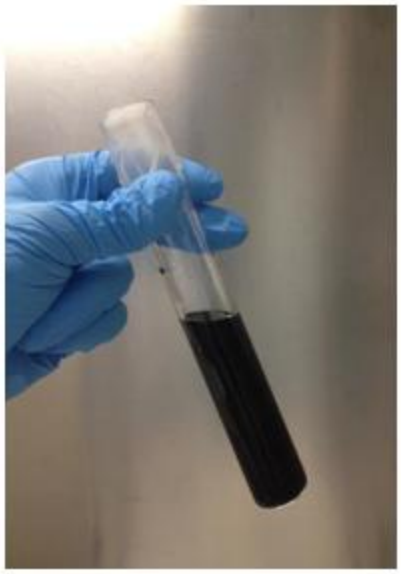

Figure S1: As synthesized suspension of PtNi(Mo)/C nanoparticles.

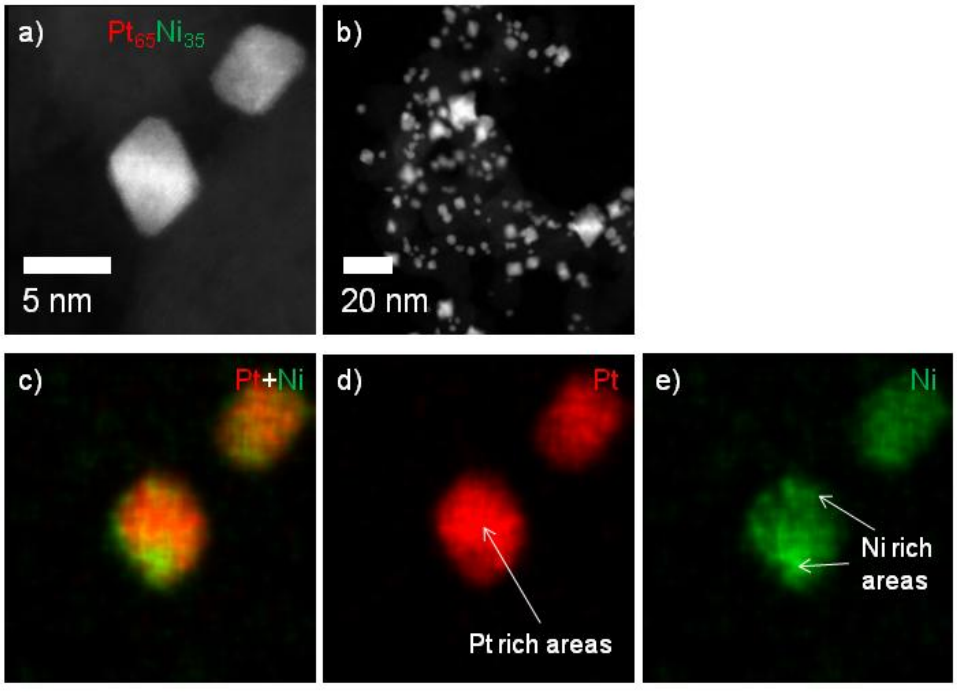

Figure S2: As prepared PtNi/C. HAADF-STEM image of two PtNi octahedral nanoparticles (a), HAADF-STEM overview image (b) and STEM-EDX composition maps (c-e) of PtNi octahedral nanoparticles from as prepared sample. Pt (red) and Ni (green) combination (c), singular Pt (d) and Ni (e) maps are shown. Composition of the nanoparticles in the images a), c), d) and e) as determined by EDX is inserted in a). Pt rich and Ni rich areas are indicated by arrows.

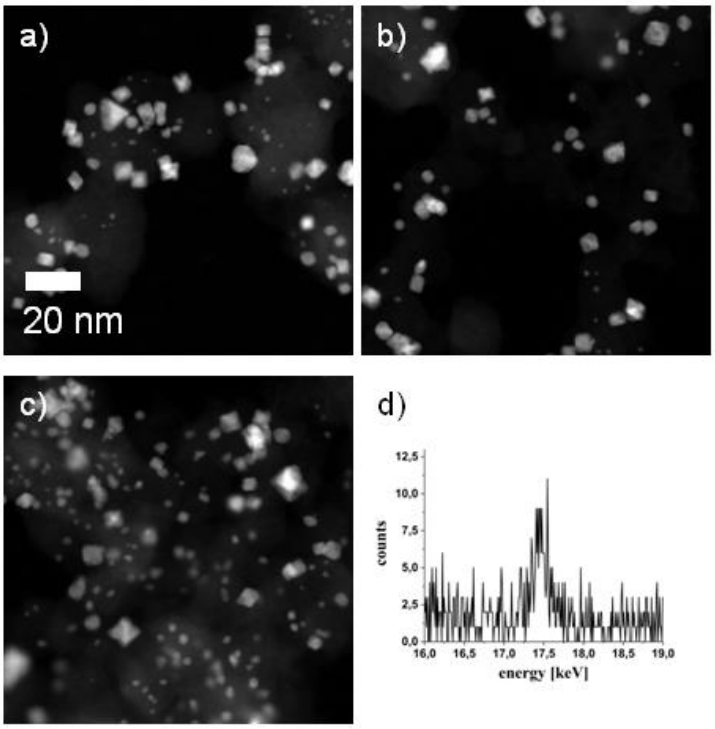

Figure S3: As prepared PtNi(Mo)/C. HAADF-STEM overview images (a-c) and intensity of Mo K-alpha peak by STEM-EDX (d).

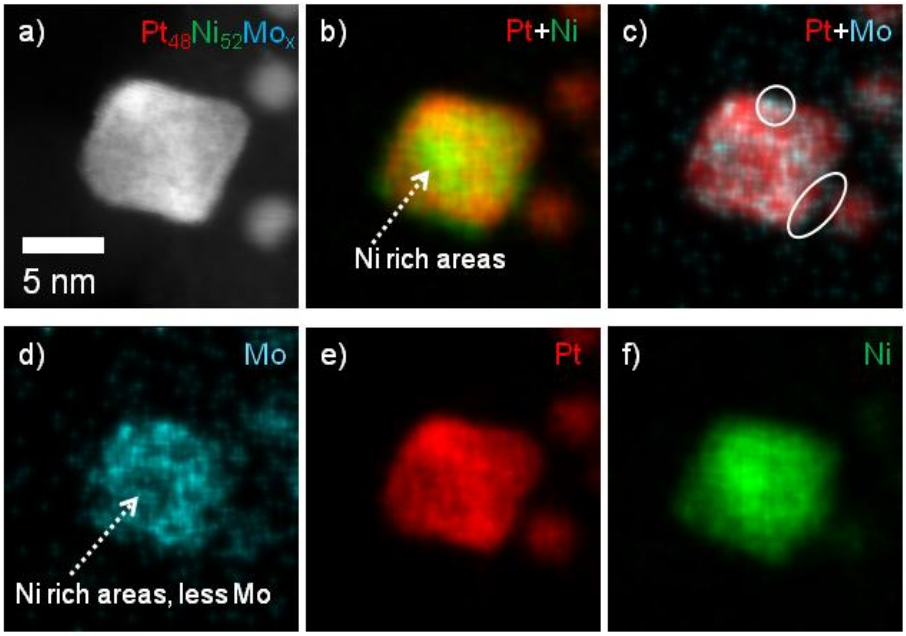

Figure S4: HAADF-STEM image (a) and STEM-EDX composition maps (b-f) of a PtNi(Mo) octahedral nanoparticle from an as prepared sample. Combined Pt (red) and Ni (green) map (b), combined Pt and Mo (cyan) map (c) and single Mo (d), Pt (e) and Ni (f) maps are shown. The EDX composition of the nanoparticle is inserted in (a). Pt rich and Ni rich areas are indicated by arrows, while circles highlight Mo enrichment at the edge of the nanoparticle.

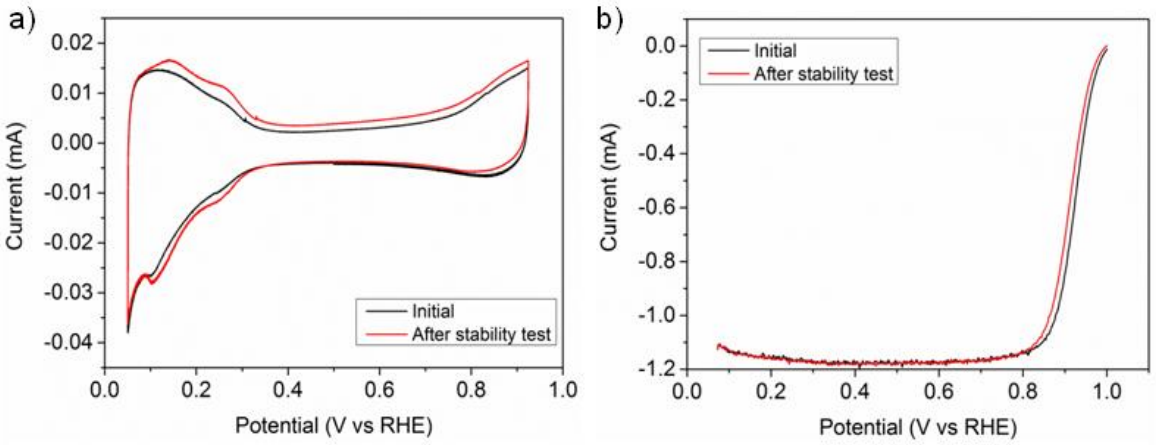

Figure S5: Electrochemical characterization, ORR activity and stability of oh-PtNi/C. Cyclic voltammetry (a) and linear sweep voltammetry (b) after activation (black) and after stability test (red) for oh-PtNi/C. Both CV and LSV were obtained at 20 mVs^{-1} and 0.1 M $HClO_4$ electrolyte. In a) the electrolyte was saturated with N_2 and rotation equal to 0 rpm, while in b) saturation with O_2 and 1600 rpm was used.

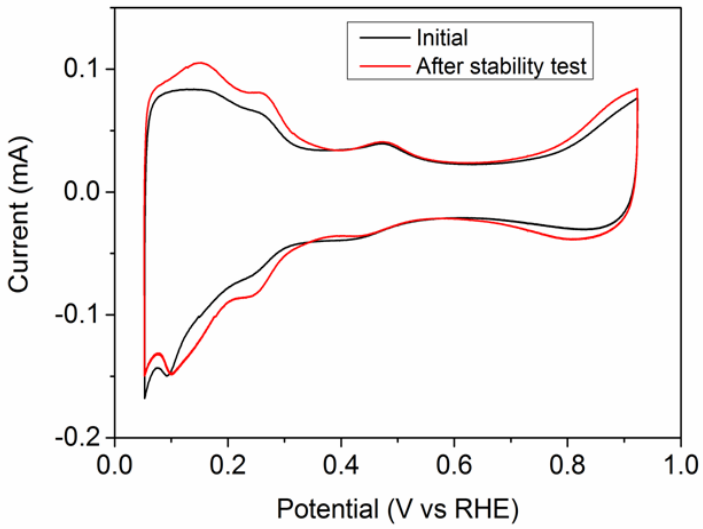

Figure S6: Mo redox peak in PtNi(Mo)/C. Cyclic voltammetry after activation (black) and after stability test (red) for oh-PtNi(Mo)/C with high Pt loading (48 μg_{Pt} cm^{-2}). Curves obtained at 20 mVs^{-1} and 0.1 M $HClO_4$ electrolyte which was saturated with N_2. RDE rotation set equal to 0 rpm.

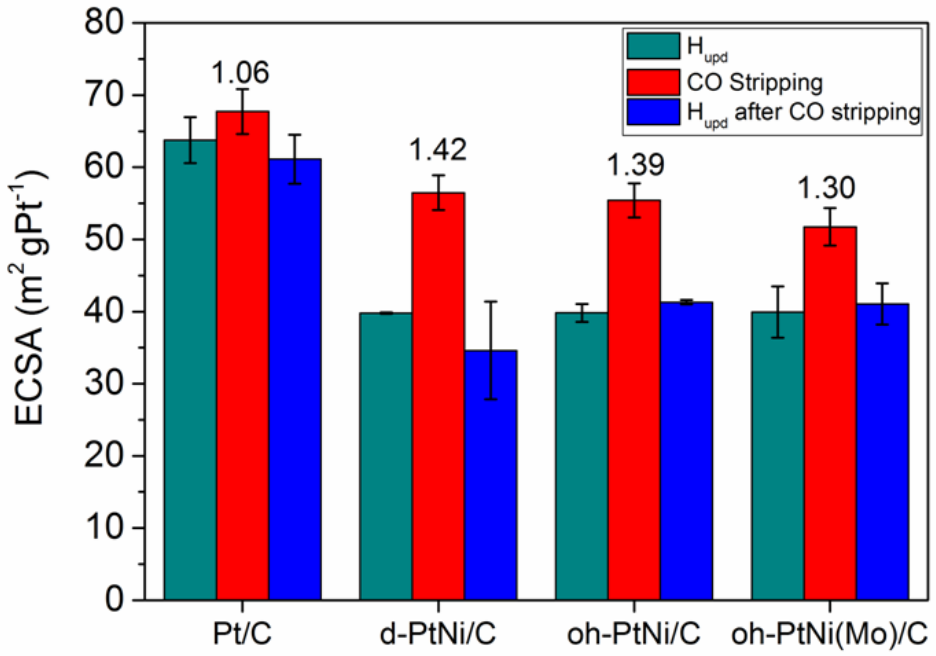

Figure S7: ECSA based on CO stripping (red) for activated Pt/C, d-PtNi/C, oh-PtNi/C and oh-PtNi(Mo)/C. For comparison the ECSA values based on H_{upd} obtained before (green) and after (blue) the CO stripping are shown. The error bars represent standard deviation from average between values obtained with different electrodes. The ratio between CO-ECSA and H_{upd}-ECSA (before CO stripping) is shown on top of the CO stripping data. All the respective potential cycles were performed at 20 mVs^{-1} in N_2 saturated electrolytes and no rotation.

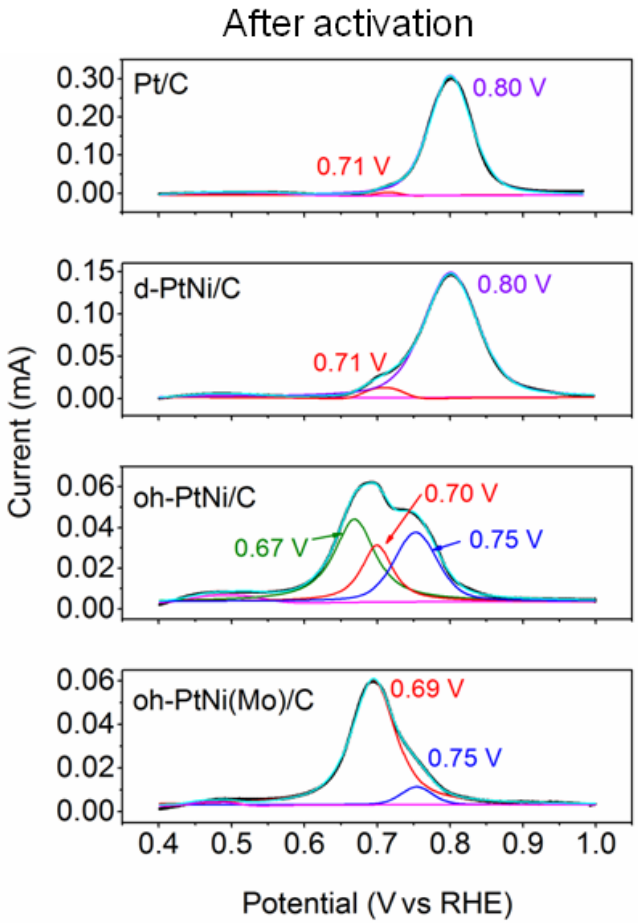

Figure S8: CO stripping curves at 20 mVs^{-1} in N_2 saturated electrolytes and no rotation obtained after activation and shown after background subtraction from 0.4 to 1.0 V_{RHE} for the same catalysts (black). The peaks were fit by pseudo-Voigt functions, fit peak contributions are shown in different colors (blue, red, green, violet and pink) while the cumulative curve is shown in cyan.

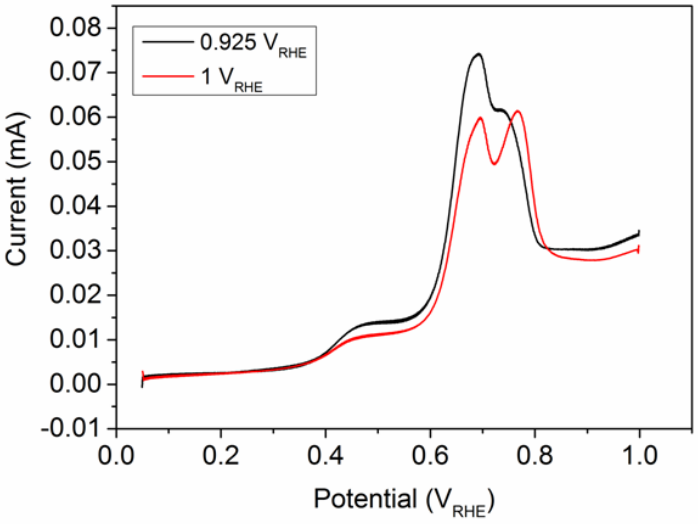

Figure S9: CO stripping for oh-PtNi/C obtained after activation by cycling the potential from 0.6 V_{RHE} to 0.925 V_{RHE} (black) and 1 V_{RHE} (red).

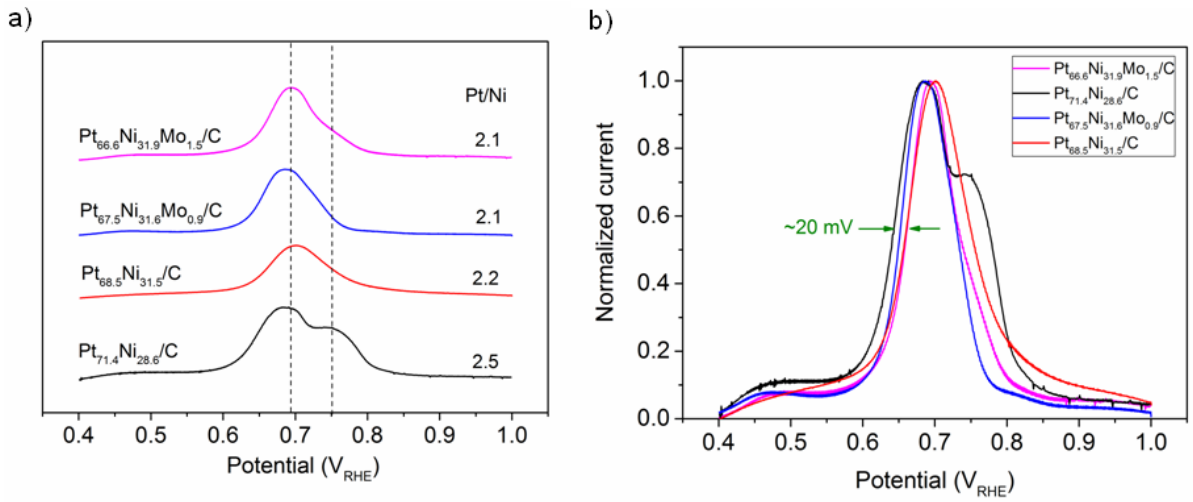

Figure S10: CO stripping curves at 20 mVs^{-1} in N_2 saturated 0.1 M $HClO_4$ electrolyte and no rotation obtained after activation and shown after background subtraction from 0.4 to 1.0 V_{RHE} for several catalysts. a) From top to bottom: oh-PtNi(Mo)/C (pink), oh-PtNi(Mo)-30wt%/C (blue), oh-PtNi/C-2steps (red), oh-PtNi/C (black). The composition as determined by ICP-OES is shown next to the corresponding curves as well as the Pt/Ni ratio. Two vertical dashed lines highlight the position of the two main contributions. b) Same curves showed after normalization to emphasize possible shifts. In the case of these four catalysts the shift is small, as indicated in green.

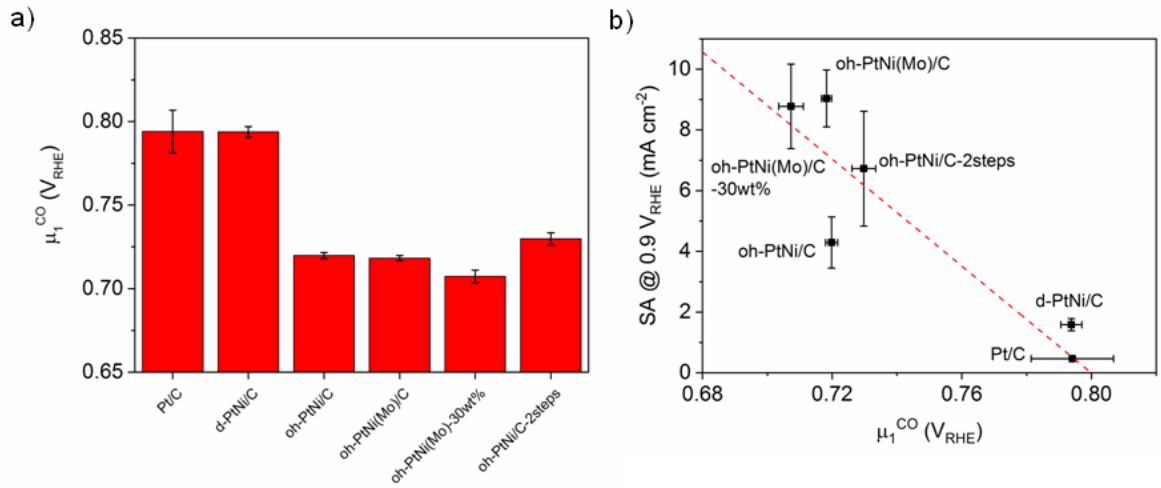

Figure S11: The first moment of the potential weight (μ_1^{CO}) of the CO stripping voltammogram obtained in the range 0.4-1.0 V_{RHE} for Pt/C, d-PtNi/C, oh-PtNi/C, oh-PtNi(Mo)/C, oh-PtNi(Mo)-30wt%/C and oh-PtNi/C-2steps (a). The error bars represent standard deviations from average between values obtained with different electrodes. Specific activity based on H_{upd}-ECSA and evaluated at 0.9 V_{RHE} plotted as a function of μ_1^{CO} for the same samples (b). The dashed red line is a linear fit of the entire set of data. The error bars associated with SA values represent standard deviations obtained by error propagation of the standard deviations of the mass activity (MA) and H_{upd}-ECSA.

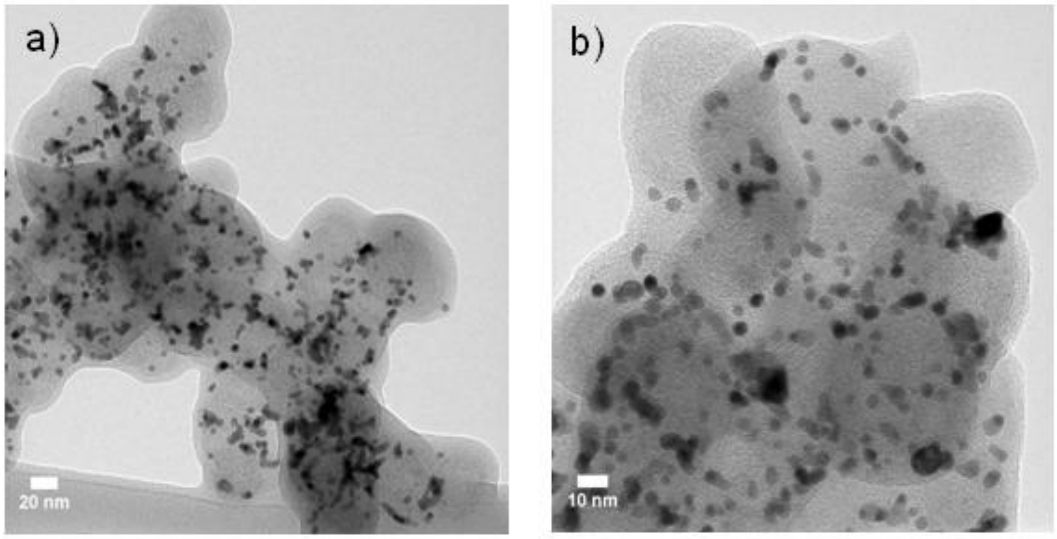

Figure S12: TEM images of PtNi/C after the stability test with a RDE.

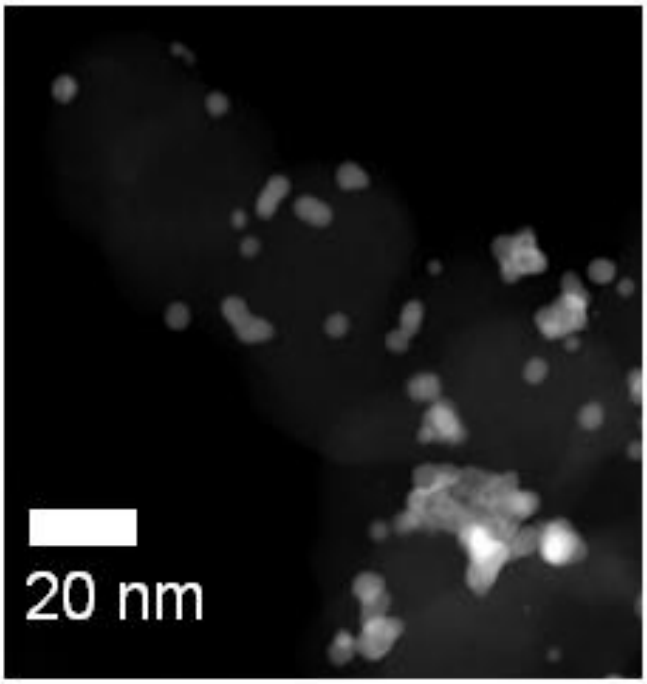

Figure S13: HAADF-STEM overview image of PtNi(Mo)/C after the stability test in a RDE.

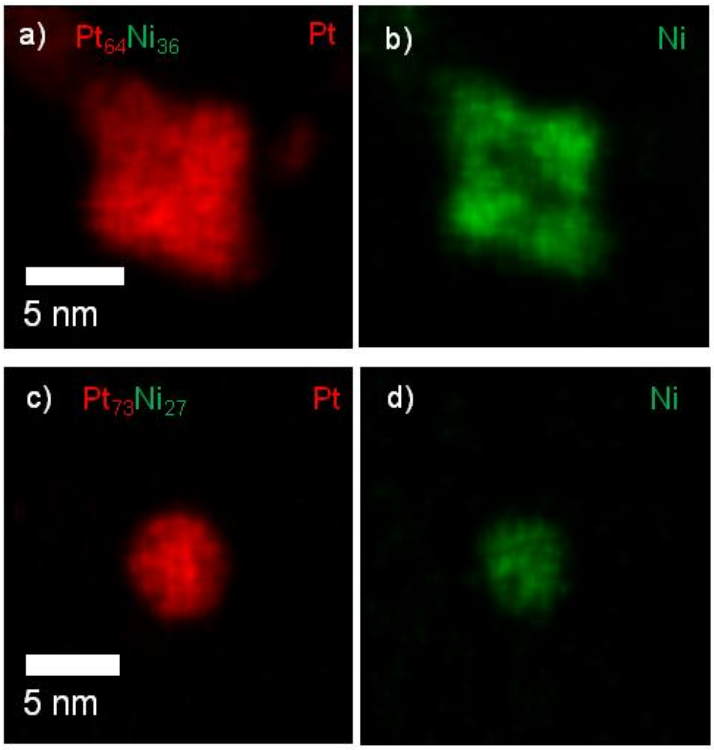

Figure S14: STEM-EDX single element composition maps (b-d) of PtNi(Mo)/C particles shown in Figure 3e-h after the stability protocol conducted using a RDE. A concave octahedral is shown in a) and b) while a pseudospherical particle is shown in c) and d), corresponding to the STEM-EDX and HAADF-STEM shown in Figure 3e-h. Pt is shown in red and Ni in green. The nanoparticle composition is inserted in a) and c).

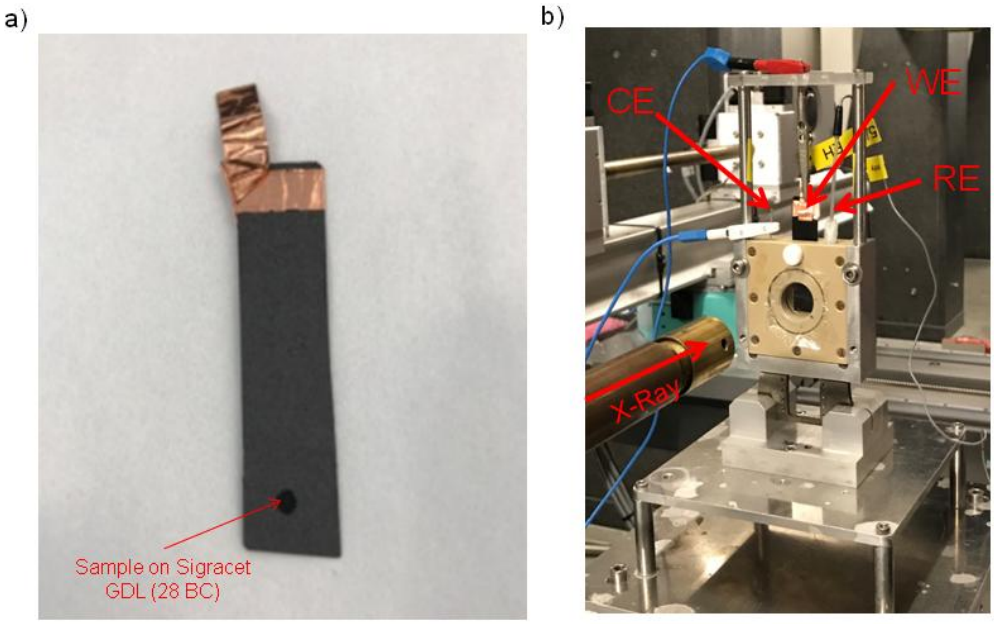

Figure S15: Working electrode prepared for *in situ* WAXS measurements (a). The sample is indicated by a red arrow. Electrochemical setup for *in situ* WAXS (b). The counter electrode (CE), working electrode (WE) and reference electrode (RE) are indicated with a red arrow, as well as the direction of the incident X-ray beam.

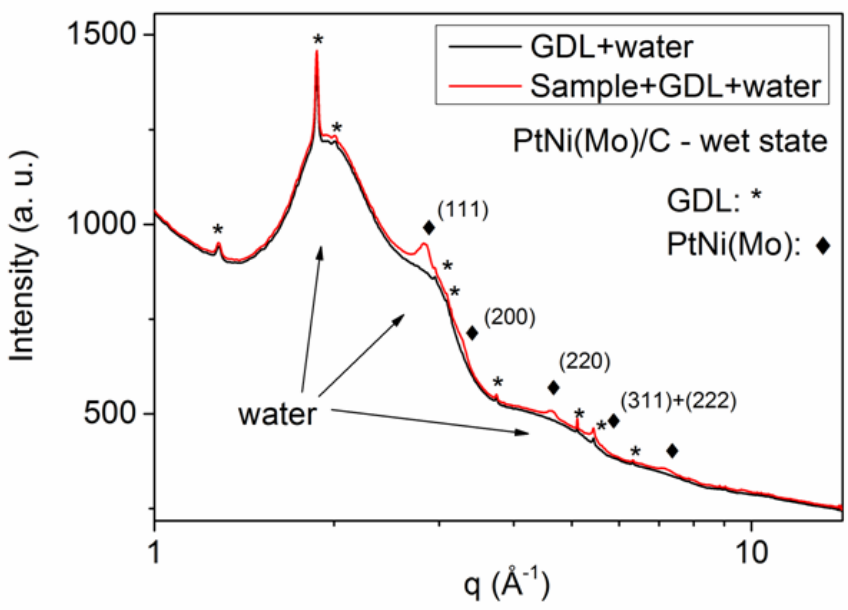

Figure S16: *In situ* WAXS patterns as integrated after collected by the 2D detector of PtNi(Mo)/C in the cell filled with electrolyte (wet state) (red) and background position consisting of a GDL area without sample (black). The broad water reflection are indicated by black arrows, the reflections associated to fcc Pt-based alloy are indicated by a rhombus (♦) and labeled, while the sharp reflection of the GDL are indicated by an asterisk (*). On this scale the broad and weak reflections of the carbon support are not visible.

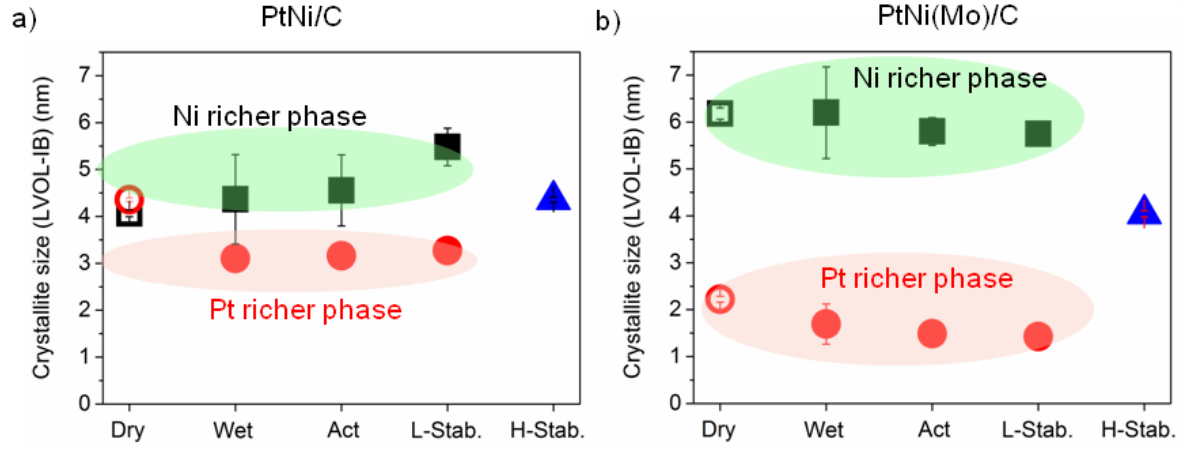

Figure S17: Size of coherently scattering domains for PtNi/C (a) and PtNi(Mo)/C (b) calculated from the integral breadth by Rietveld refinement of the *in situ* WAXS patterns (full symbols) and laboratory XRD (open symbols). Data points are shown for the dry state, wet state, activated state, after L-stability and after H-stability. For the first four states a two phase composition shows the best fit and the two phases are indicated as Pt rich phase (red dots) and Ni rich phase (black squares). Pink and green ovals highlight the similarity of the phases among the three states. For H-stability a single phase was used in the fit (blue triangles). Error bars represent standard deviations provided by Topas for the refined parameters.

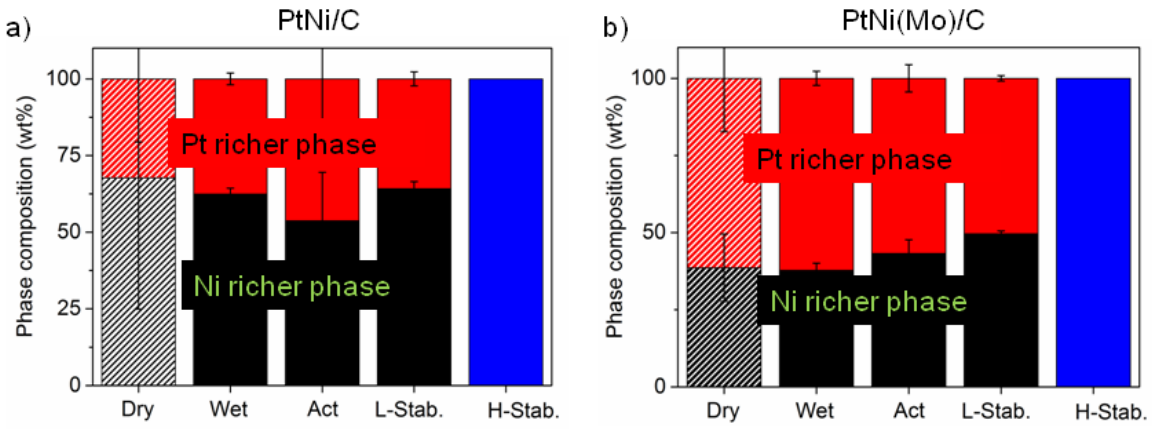

Figure S18: Phase composition in weight percentage for PtNi/C (a) and PtNi(Mo)/C (b) from Rietveld refinement of the *in situ* WAXS patterns (full) and laboratory XRD (dashed) and measured for the dry state, wet state, activated state, after L-stability and after H-stability. For the first three states a two phase composition shows the best fit and the two phases are indicated as Pt rich phase (red) and Ni rich phase (black). For H-stability a single phase was used in the fit (blue squares). Error bars represent standard deviations provided by Topas for the refined parameters.

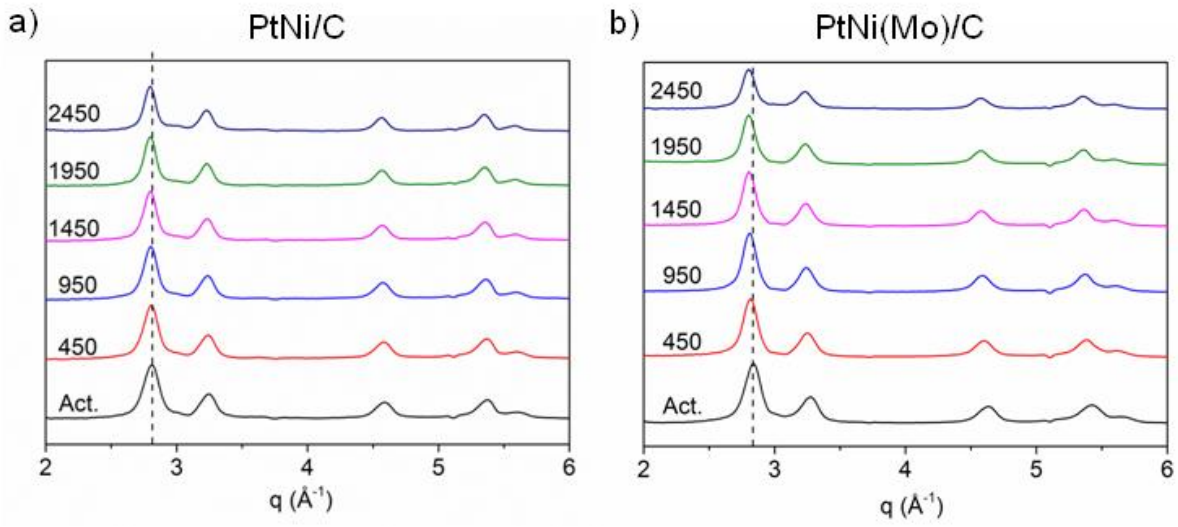

Figure S19: In situ WAXS patterns obtained during H-stability test for PtNi/C (a) and PtNi(Mo)/C (b). The numbers on the left of the figures correspond to the potential cycle number associated to the pattern. The pattern of the activated state (Act.) is also shown. Vertical dashed lines are guides to the eye.

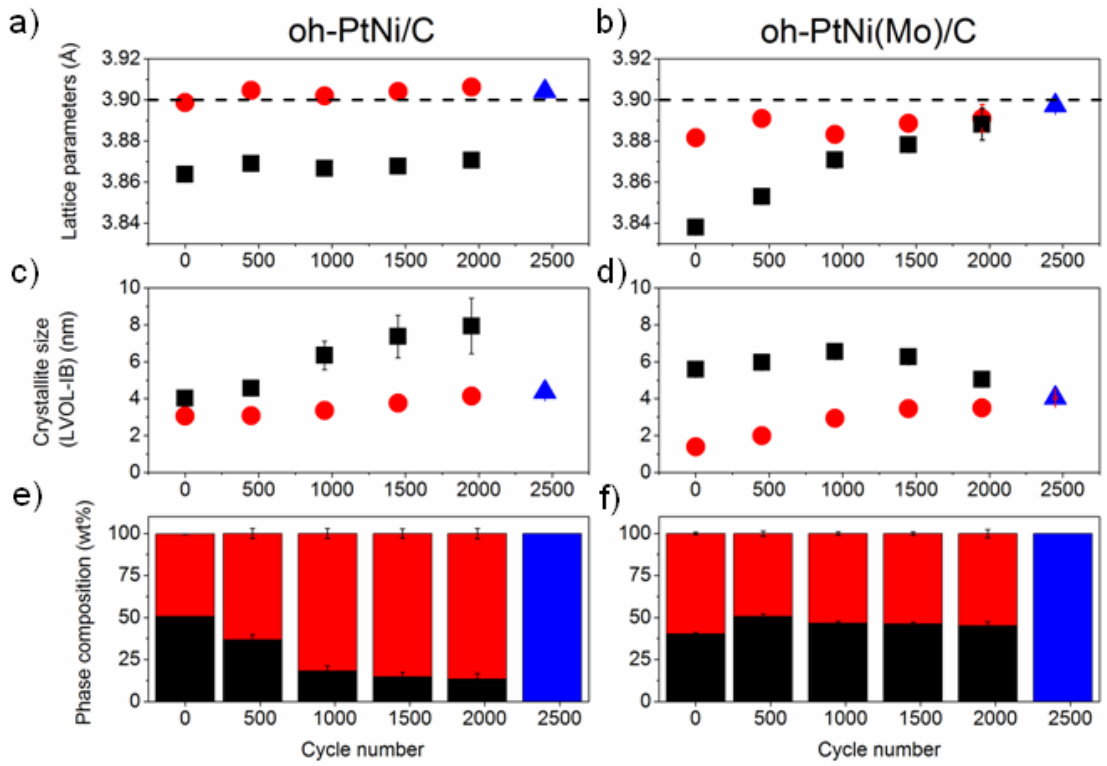

Figure S20: Results of Rietveld refinement of *in situ* WAXS patterns obtained during H-stability test for PtNi/C (a, c, e) and PtNi(Mo)/C (b, d, f). The results include the lattice parameter (a, b), the size of the coherently scattering domains (c, d) and the phase composition (e, f). The horizontal dashed line in a) and b) at the lattice parameter of 3.90 Å is intended as a guide to the eye. The same color code and symbols as in Figure S17-S18 is used to differentiate the different phases. Error bars represent standard deviations provided by Topas for the refined parameters.

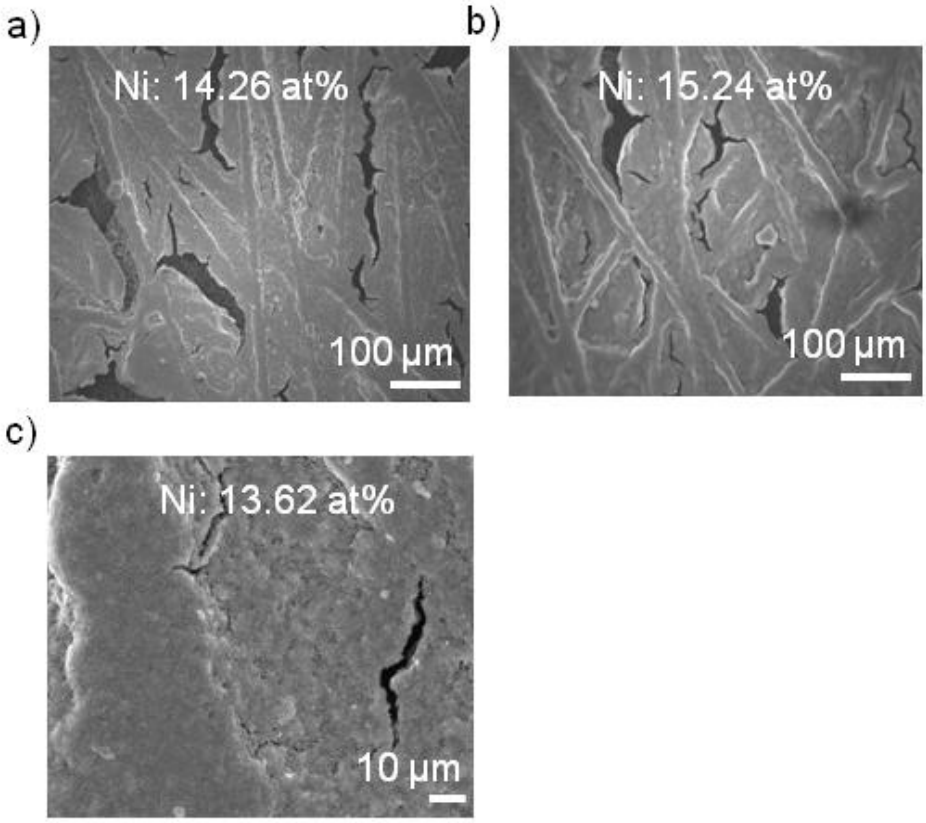

Figure S21: SEM images of PtNi/C on GDL after H-stability protocol of three different areas at 200x magnification (a, b) and 1000x (c). The content of Ni measured by SEM-EDX is shown for each image.

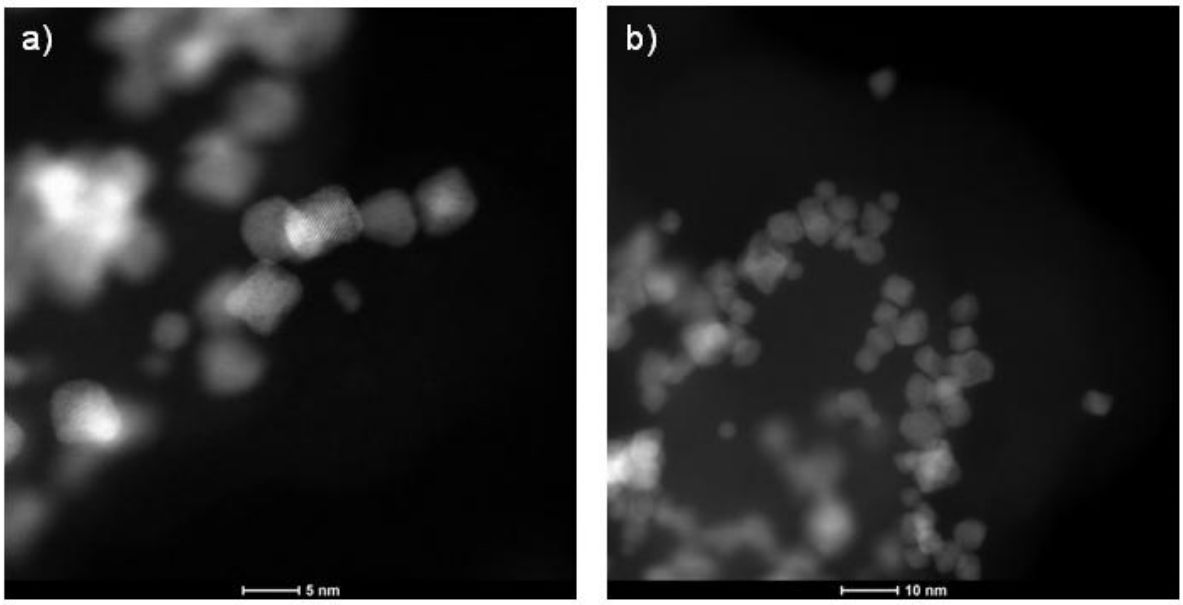

Figure S22: HAADF-STEM overview images of PtNi(Mo)/C after H-stability test.

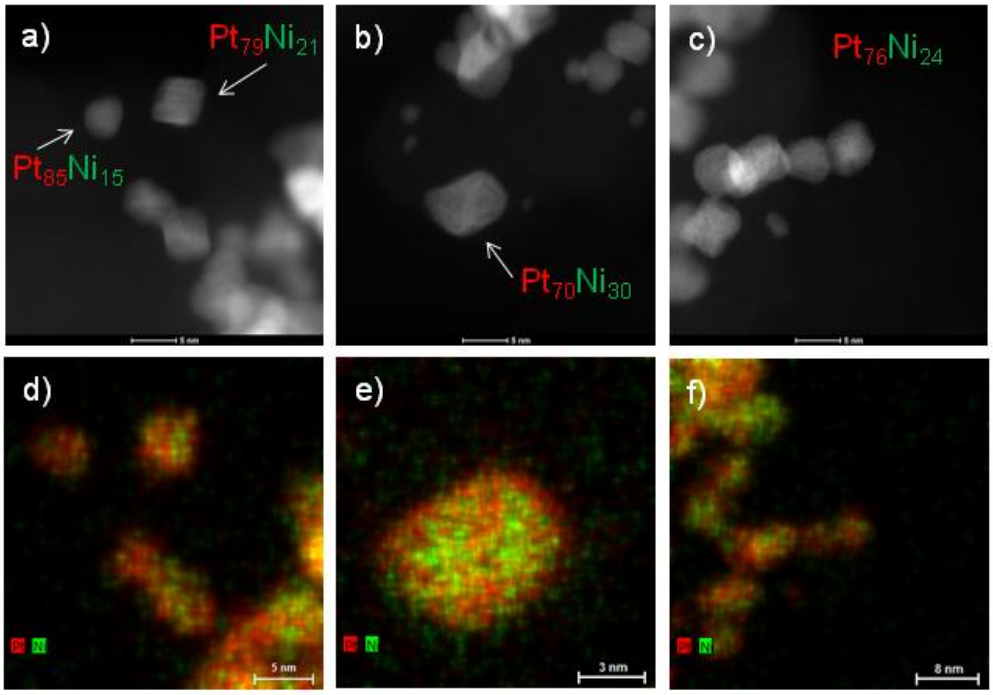

Figure S23: HAADF-STEM images (a-c) and associated STEM-EDX composition maps (d-f) of PtNi(Mo)/C after the H-stability test showing the Pt (red) and Ni (green) element distribution. The composition as determined by EDX is inserted in (a-c). White arrows indicate the specific nanoparticles for which the composition is measured.

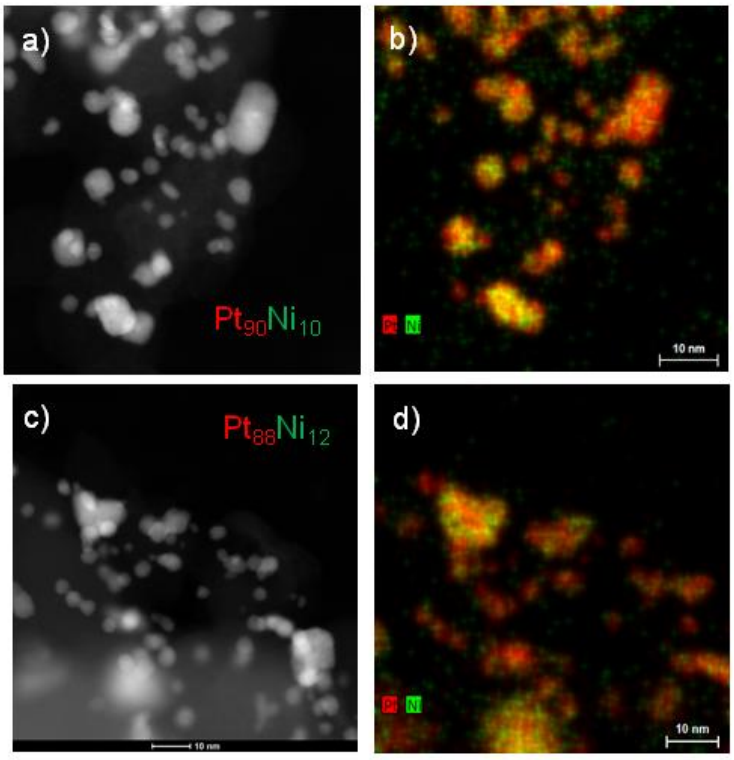

Figure S24: HAADF-STEM images (a, c) and associated STEM-EDX composition maps (b, d) of PtNi/C after the H-stability test showing the Pt (red) and Ni (green) element distribution. The composition as determined by EDX is inserted in (a, c).

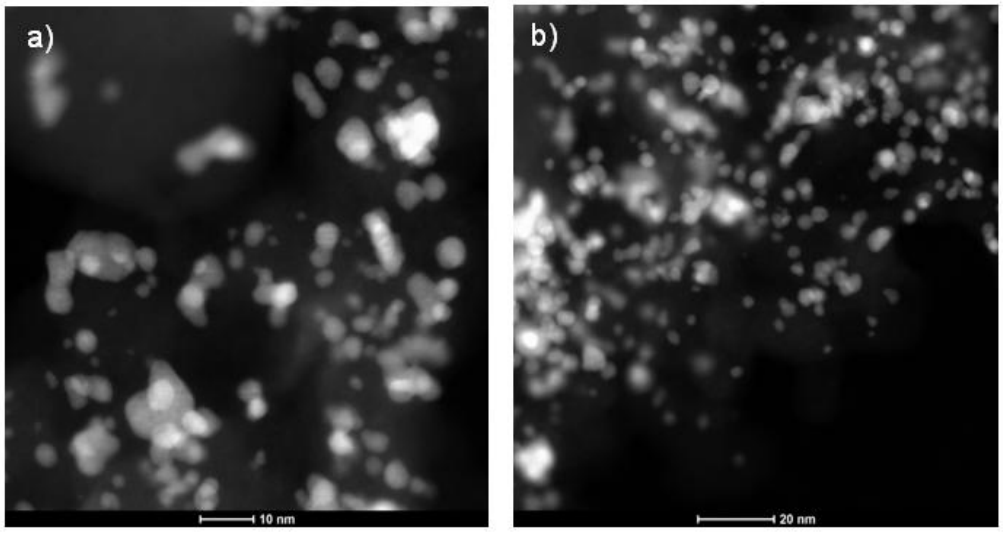

Figure S25: HAADF-STEM overview images of PtNi/C after H-stability test.

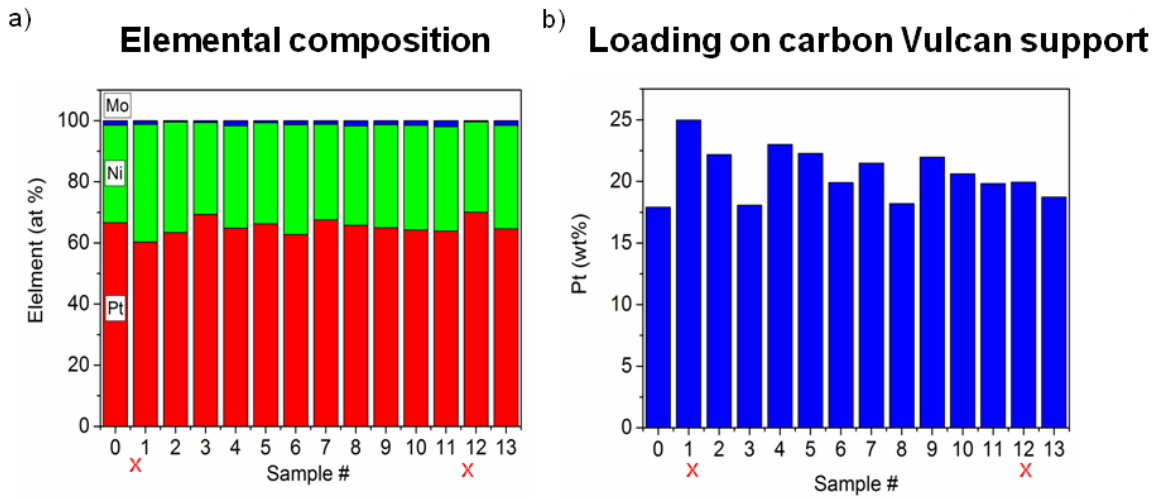

Figure S26. Elemental composition (a) and Pt based weight loading on carbon support (b) for the PtNi(Mo)/C replicas. In a) the atomic content of Mo (blue), Ni (green) and Pt (red) is shown. The two red Xs indicate the samples which have been discarded. The values of the reference oh-PtNi(Mo)/C have been included for comparison and the sample is labeled as sample 0.

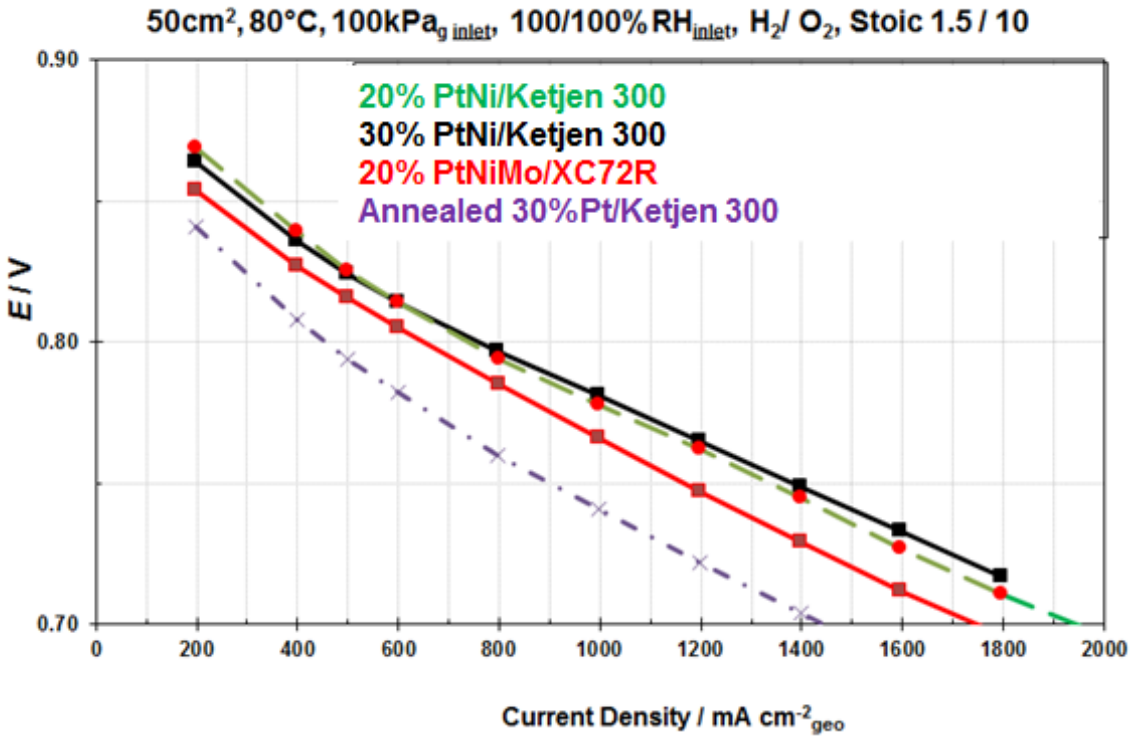

Figure S27. Polarization curves as function of current density for MEA single cell measurements with oh-PtNi(Mo)/C (red), 20 Pt wt% and 30 Pt wt% d-PtNi/C (green and black, respectively) and annealed 30 Pt wt% Pt/C (violet) as cathode and Pt/C as anode in H_2/O_2. All catalysts were tested with the same cathode loading, 0.1 $mg_{Pt}\,cm^{-2}$. The loading for the anode was 0.1 $mg_{Pt}\,cm^{-2}$. Other experimental conditions are reported above the plots. The particle size of the annealed 30 Pt wt% Pt/C is ~ 7 nm, which is comparable to the average size of the oh-PtNi(Mo)/C. The mass activity at 0.9 V and ECSA of the annealed 30 Pt wt% Pt/C are 0.15 A mg_{Pt}^{-1} and 45 $m^2\,g_{Pt}^{-1}$.

1. X. Q. Huang, Z. P. Zhao, L. Cao, Y. Chen, E. B. Zhu, Z. Y. Lin, M. F. Li, A. M. Yan, A. Zettl, Y. M. Wang, X. F. Duan, T. Mueller and Y. Huang, *Science*, 2015, **348**, 1230-1234.
2. G. D. Niu, M. Zhou, X. Yang, J. Park, N. Lu, J. G. Wang, M. J. Kim, L. D. Wang and Y. N. Xia, *Nano Lett*, 2016, **16**, 3850-3857.
3. K. Momma and F. Izumi, *Journal of Applied Crystallography*, 2011, **44**, 1272-1276.
4. S. Martens, L. Asen, G. Ercolano, F. Dionigi, C. Zalitis, A. Hawkins, A. M. Bonastre, L. Seidl, A. C. Knoll, J. Sharman, P. Strasser, D. Jones and O. Schneider, *J Power Sources*, 2018, **392**, 274-284.
5. R. Chattot, T. Asset, P. Bordet, J. Drnec, L. Dubau and F. Maillard, *Acs Catal*, 2017, **7**, 398-408.
6. T. Asset, R. Chattot, J. Drnec, P. Bordet, N. Job, F. Maillard and L. Dubau, *Acs Appl Mater Inter*, 2017, **9**, 25298-25307.
7. C. H. Cui, L. Gan, M. Heggen, S. Rudi and P. Strasser, *Nat Mater*, 2013, **12**, 765-771.
8. P. Strasser, *Science*, 2015, **349**, 379-380.
9. L. García-Cruz, V. Montiel and J. Solla-Gullón, *Phys. Sci. Rev.*, 2019, **4**, 34.
10. A. Kongkanand and M. F. Mathias, *J Phys Chem Lett*, 2016, **7**, 1127-1137.

11. N. Becknell, Y. J. Kang, C. Chen, J. Resasco, N. Kornienko, J. H. Guo, N. M. Markovic, G. A. Somorjai, V. R. Stamenkovic and P. D. Yang, *J Am Chem Soc*, 2015, **137**, 15817-15824.
12. S. Rudi, C. H. Cui, L. Gan and P. Strasser, *Electrocatalysis-Us*, 2014, **5**, 408-418.
13. D. F. van der Vliet, C. Wang, D. G. Li, A. P. Paulikas, J. Greeley, R. B. Rankin, D. Strmcnik, D. Tripkovic, N. M. Markovic and V. R. Stamenkovic, *Angew Chem Int Edit*, 2012, **51**, 3139-3142.
14. L. Wang, W. P. Gao, Z. Y. Liu, Z. H. Zeng, Y. F. Liu, M. Giroux, M. F. Chi, G. F. Wang, J. Greeley, X. Q. Pan and C. Wang, *Acs Catal*, 2018, **8**, 35-42.
15. V. Beermann, M. Gocyla, S. Kuhl, E. Padgett, H. Schmies, M. Goerlin, N. Erini, M. Shviro, M. Heggen, R. E. Dunin-Borkowski, D. A. Muller and P. Strasser, *J Am Chem Soc*, 2017, **139**, 16536-16547.
16. R. M. Aran-Ais, F. J. Vidal-Iglesias, M. J. S. Farias, J. Solla-Gullon, V. Montiel, E. Herrero and J. M. Feliu, *J Electroanal Chem*, 2017, **793**, 126-136.
17. J. Solla-Gullon, F. J. Vidal-Iglesias, E. Herrero, J. M. Feliu and A. Aldaz, *Electrochem Commun*, 2006, **8**, 189-194.
18. K. J. J. Mayrhofer, M. Arenz, B. B. Blizanac, V. Stamenkovic, P. N. Ross and N. M. Markovic, *Electrochim Acta*, 2005, **50**, 5144-5154.
19. T. R. Garrick, T. E. Moylan, V. Yarlagadda and A. Kongkanand, *J Electrochem Soc*, 2017, **164**, F60-F64.
20. A. Cuesta, A. Couto, A. Rincon, M. C. Perez, A. Lopez-Cudero and C. Gutierrez, *J Electroanal Chem*, 2006, **586**, 184-195.